Journal of Imaging Science and Technology® 66(5): 050404-1–050404-11, 2022.

Statistical Analysis of Sparkle in Snow Images

Mathieu Nguyen▲, Jean-Baptiste Thomas▲, and Ivar Farup▲
Department of Computer Science, Norwegian University of Science and Technology (NTNU), Norway
E-mail: mathieu.nguyen@ntnu.no

Abstract. *Sparkle from snow is a common phenomenon in Nature but not well studied in the literature. We perform a statistical study on digital snow images captured in-situ to analyze sparkle events by using contrast and density of sparkle spots descriptors. The method for measuring sparkles by Ferrero et al. is adapted, tested, and verified to the case of snow. The dataset is divided into three categories representing the type of snow acquired: dense snow, fresh snow, and old snow. Our analysis highlights the link between the sparkle of snow, the nature of snow and its grain structure. Sparkle could thus be a feature used for snow classification.*

[DOI: 10.2352/J.ImagingSci.Technol.2022.66.5.050404]

1. INTRODUCTION

Snow is not only a nice and cold white surface, but also a complex material with a specific structure. In Nature, one may have a richer experience, such as various chromatic phenomena happening on the snow surface when illumination and observation conditions are met. This paper focuses on one of those particular visual phenomena: the sparkle of snow.

Snow is a complex material and its perception calls on several external factors. More specifically, snow is made of grains whose structure can be represented by two main quantities as defined by Fierz et al. [1]: the snow grain shape which describes the morphological form of snow grains, and the snow grain size. Studies have been conducted to identify shape factor and study the influence of the grain shape on the quantity of light in snow media and are reported in the literature [2, 3], others have used close-range imaging or remote sensing to obtain estimates of snow grain sizes [4–7].

To our knowledge, the sparkle effect generated by snow has not been covered specifically in any academic work. Yet it is possible to find work on the generation of snow sparkle. There have been few attempts in the computer graphics area with Wang et al. [8]. They worked on a stochastic model to simulate sparkle spots in real-time for virtual snow scenes used in the video game industry. Other references such as Jakob et al. [9] or Wang et al. [10] mention the case of snow in their work, and they test their rendering model with this natural material. However, none of those rendering models for sparkle are physically-based and therefore do not take into consideration the nature of the snow material and its complexity due to various parameters such as temperature, pressure, snow grain shape and snow grain size.

In ASTM E284-17 Standard Terminology of Appearance [11], sparkle is defined as "the aspect of the appearance of a material that seems to emit or reveal tiny bright points of light that are strikingly brighter than their immediate vicinity and are made more apparent when a minimum of one of the contributors (observer, specimen, light source) is moved". This definition can be referenced as the visual sparkle which can be experienced by a human observer. However, the sparkle considered in this article would be close to an imaging sparkle as it is observed through the scope of a digital camera. The term imaging sparkle refers to a pixel source whose values are maxima and higher to pixel values of its near surrounding. Thus, sparkle is considered as a pixel point and not an accumulation of pixels. Moreover, even though the visual and imaging sparkle are defined differently, they are linked. Assessing the presence of visual sparkle on a scene would likely lead to the detection of imaging sparkle.

Sparkle, as a texture effect, has been described in detail in various models in the case of metallic paintings or surfaces. One of the first models introduced was done by Ershov et al. [12] where they presented a computational procedure to obtain sparkle texture for image rendering. Another model introduced by Kitaguchi et al. [13] used digital images taken under various exposure times to reconstruct a HDR image and make an estimate of sparkle points. In the literature, two models can be described: models which generate visible sparkle on images [9, 14], and models analyzing images to measure the sparkle present on them [13, 15].

The model proposed by Ferrero et al. [15] has been chosen for its easy computational implementation and the use of the *in-situ* images of the dataset. The paper introduces a model for graininess and sparkle, both considered as texture effects. These effects are then linked to parameters of the optical system used for recording or capturing, the illumination and observation conditions, and the coating parameters of surfaces studied. This model concludes by introducing two variables to study when it comes to characterizing sparkle. First, the contrast of sparkle spots is considered and is related to specular reflectance of the flakes and their size, and to the diffuse reflectance of coatings. The second variable is the density of sparkle spots, which is correlated to the orientation distribution of flakes and their flatness.

Following this model, Ferrero et al. developed a procedure to measure quantities of well-defined sparkle

▲ IS&T Members.

Received May 15, 2022; accepted for publication July 26, 2022; published online Aug. 11, 2022. Associate Editor: Samuel Morillas.
1062-3701/2022/66(5)/050404/11/$25.00

measurands [15], with experimental results obtained from combinations of several illuminations and viewing geometries. This work also presents four descriptors characterizing sparkle distributions and correlated to visual attributes:

- the maximum contrast value of sparkle spots to ensure the Human Visual System is able to distinguish sparkle spots from the background,
- the maximum density of sparkle spots,
- the visibility inconstancy linked to the variation of contrast values due to illumination and viewing geometries,
- the anisotropy referring to the variation of density of sparkle with illumination and viewing conditions.

While these four descriptors can be linked to visual attributes, the last two of them are tightly correlated with illumination and viewing conditions, meaning they will vary from scene to scene as the environment changes.

Ferrero et al. pursued their work on sparkle with two other studies. Measurements of sparkle were performed on several samples with different coatings, illumination and viewing conditions at various institutes [16]. They used similar indicators (visibility and density of sparkle spots) to describe those texture events, and the algorithm used for detection and estimation of those indicators was presented. In this work, they also identified two potential sources of errors while characterizing the sparkle: inadequate illumination and collection of solid angles, and a wrong aperture size chosen on the optical tool used for observing the sparkle spots. Finally, their work [17] highlights the method they developed over the years, few measurement scales for sparkle and graininess and their correlation with subjective evaluations.

This article presents a dataset of digital snow images which are all acquired *in-situ* and show visual sparkle events on them. Then, a statistical study of sparkle spots on this dataset is conducted by following the method of Ferrero et al., and using the indicators provided by it. The results of this study are used to discuss the potential correlation between the sparkle spots on snow and the snow grain structure with descriptors such as the snow grain shape and the snow grain size. The goal is to verify if the method developed by Ferrero et al. can be used for the case of snow. Results of these statistical studies lead to designing a precise acquisition protocol to identify the snow grain shape, and make links between sparkle events and snow grain classification.

The article first introduces the methodology used for the acquisition of images, a description review of the dataset, and the preprocessing applied to the images before dealing with the algorithm of sparkle detection. The second section provides the results computed, the observations and interpretations, and their links to the snow structure. The last part concludes the article and presents future works.

2. METHODOLOGY

2.1 *Dataset and Acquisition of Images*

The dataset is composed of 492 images in total and can be divided with the following distribution: 452 images were acquired during daytime and with uncontrolled illumination, and 40 images were captured at night with a torchlight as a source of illumination. All images were registered in RGB RAW format and their size is 3936 × 2624 pixels. Table I is presenting the different types of snow composing the dataset and the dates of acquisition for images. Figure 1 is displaying some examples of images composing the dataset.

Table I. Description of snow content of the dataset.

Dates of acquisition	Types of snow	Number of images
02.06.2022–02.08.2022	Dense snow	263
02.15.2022	Fresh snow	47
03.18.2022–04.11.2022	Old snow	182

Acquisitions were performed between February 2022 and April 2022 in Norway, where our department is located. A major aspect of this dataset is that all images used were taken outside in uncontrolled conditions. It means the snow was left untouched with appropriate temperature and pressure conditions, and it was not changed due to a move in a cold room inside. Snow metamorphism [1] is a phenomenon causing snow to change based on external and mechanical properties. Thus, having kept snow in its natural state is a strength of this dataset. Acquisitions were made with a Nikon D610 DSLR camera, producing RGB images. Combined with this camera was a Sigma DG Macro lens with focal lengths varying from 28 mm to 300 mm and aperture between f/3.5 and f/6.3. The camera was mounted on a tripod and was oriented to observe the scene such as the two configurations shown in Figure 2.

Illumination and viewing conditions also vary for images within the dataset. 310 images were acquired with an elevation angle of 30° for the camera, and 182 images were captured with the camera facing orthogonally to the scene (i.e. an elevation angle of 0°). Setups used could be similar to a Reflectance Transformation Imaging (RTI) setup. Here, RTI was not possible due to lack of tools to go outside in the snow to perform such acquisitions. Also, the setup used offered more flexibility to test the algorithm proposed by the work of Ferrero et al [16]. For 452 images, the sun was the light source used as images were captured during daytime. All day images were acquired under a clear sky without clouds, meaning the sun had direct illumination on the scene. Images were taken at different exposure times to cope with strong direct illumination of some setups to avoid having oversaturated images.

In the study of sparkle, azimuth angles for incidence of light sources are commonly used as parameters. For this dataset, it was possible to estimate those angles of incidence by looking at shadows cast on some of the images, or by taking pictures of the setup with the light source visible. Hence, most angles of incidence are estimated and not precisely measured, so their uncertainty could be high. We moderate this choice by conducting a statistical study on a large dataset of images to smooth these potential

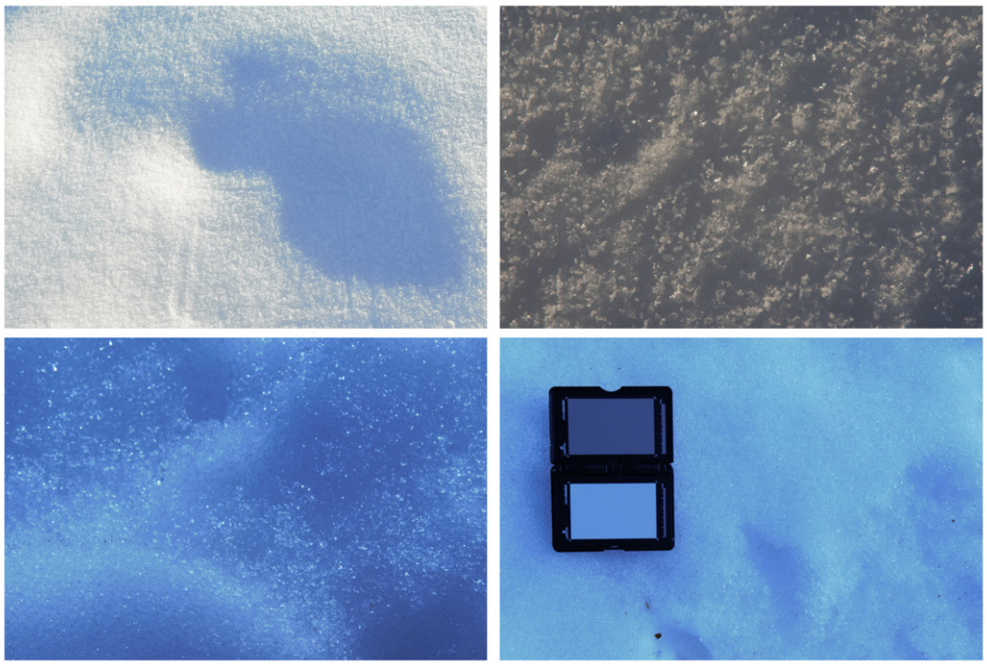

Figure 1. Examples of images in the dataset studied taken under direct illumination with different exposure times.

Figure 2. Two setups used for acquisition of snow images.

uncertainties. 3D lidar scans were made during the image acquisition process. And some images contain shadows cast on them, and for most of the scenes, global pictures were taken to ensure the presence of the sun in them. As a consequence, it is possible to have estimates of azimuth angles of the sun for those images. Furthermore, since those

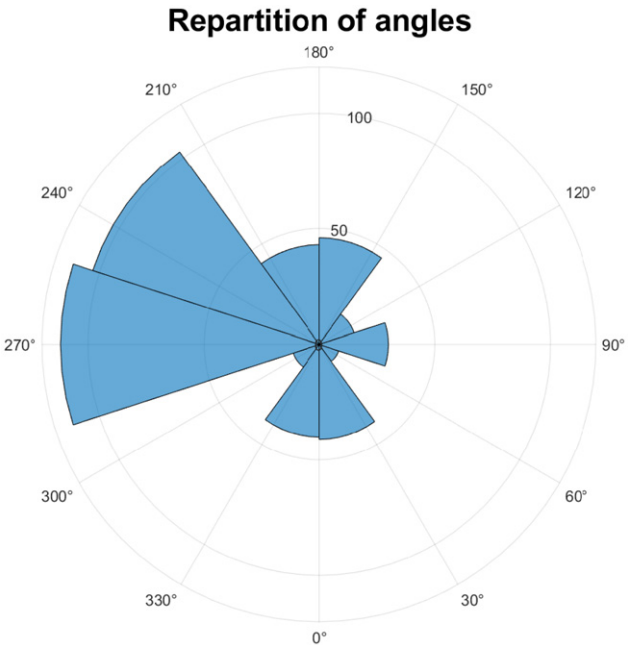

Figure 3. Repartition of incident angles for light sources in the same reference system for all images in the dataset.

images were taken from locations close to each other, and with the knowledge of 3D point clouds, all images have been replaced in the same reference system so that azimuth angles can be used for analysis and are not tied to the camera system. Regarding the 40 images captured at night, the azimuth angle of the torchlight was controlled and is known. Those images are separated from the others for the analysis as they were not acquired in the same geographic location, and then it is not possible to replace them in the same reference system. Figure 3 shows the distribution of angles put in the same reference system across the dataset of images.

2.2 *Preprocessing of Images*

Preprocessing of images is performed according to Ferrero et al. method [16]. It consists of capturing an object's image with known properties such as reflectance or luminance, then use that known information to compute a ratio in order to estimate the unknown reflectance or luminance of the rest of the scene or other objects. All of that is possible assuming the linearity of the camera, which is made in the case of this study as well. The most commonly used objects for these calibrations are white calibration tiles, which are considered Lambertian and with known reflective properties.

The case of snow is more challenging. In the visible range, snow is commonly white, and its reflective properties are higher than the traditional calibration tiles manufactured. The reason is mainly due to scattering and subsurface scattering phenomena occurring near the snow surface, so that the amount of light reflected is large. Since snow is the main target of this statistical study, the preprocessing needs to be refined because the difference between the sparkle (high pixel values or saturated pixels) and the snow (white, so high pixel values) is too narrow. In order to perform a white balance on the images, the Gray World assumption [18] is performed. Images from our dataset are RGB images. Then, the green channel is taken as the reference and the ratios computed are

$$\overline{R} = \frac{R}{G}; \overline{B} = \frac{B}{G} \tag{1}$$

to compute the assumption. Then, those 3 channels $\overline{R}$, G, $\overline{B}$ are averaged following Eq. (2)

$$I = \frac{\overline{R} + G + \overline{B}}{3} \tag{2}$$

to obtain an image of intensities I that is used to compute sparkle algorithms later described.

2.3 *Sparkle Detection and Estimation*

Algorithms for the detection of sparkle and its study were developed by Ferrero et al. along several articles [14–17]. These methods were originally designed for the use of goniometric measuring tools to ensure precise values for azimuth angles and more control over illumination and viewing conditions, but can be applied to the study case we built (with higher uncertainties). The requirements are: digital images with apparent sparkle coming from the material studied, information on azimuth angles of incident light and reference for the calibration. The following description of steps of the algorithm is coming from Ferrero et al. [16].

The first step is to calibrate images obtained to get luminance factors β for each pixel of the images. As mentioned previously, the case of snow is slightly more delicate than using traditional white calibration tiles. Therefore, after applying the Gray World assumption, luminance factors are computed for each image of the dataset (as referred in [16]). Each image of the collection is large with size of 3936×2624 pixels. Then, in an attempt to reduce computational time, smaller areas are selected from original images. Patches were selected from the center of the image to ensure a maximum of focused snow on patches and no artefacts visible that are not snow related (presence of a colour checker as seen in Fig. 1). A parameter s_{hw} controls the half-width size of the patches and can be modified to reduce or expand the area for the sparkle algorithm. Once the patches are selected, a procedure to detect sparkles spots is applied and follows those steps:

(1) Find the pixel with the highest value of luminance factor β_{sp}.
(2) Once this pixel is found, a small elementary area is selected centered around that pixel with size controlled by a parameter called l_{hw} described later.
(3) All pixels in this area surrounding the sparkle spot are averaged and give the luminance factor of the background β_{bg} of the sparkle spot. Luminance factors of the sparkle and the background are stored separately to be used later in the analysis.
(4) Pixels from the elementary area are fixed to 0.
(5) Steps (1)–(4) are iterated with the new image until all pixel values reach 0. When computing step (2) with the

selection of the elementary area, pixel values already put at zero are not considered in the computation of the average. Also, if more than two thirds of pixels in the elementary area is at 0, the area is not considered, put to zero and the algorithm goes to the next maximum of the image.

The choice of the size of elementary area l_{hw} is to be discussed as it cannot be chosen small for physical meaning, but not too large as well. Otherwise, there is a risk of avoiding some relevant sparkle spots if the distance between two consecutive spots is smaller than l_{hw}. An impact study on the choice of s_{hw} and l_{hw} has been conducted and is presented in a later part. Results of this procedure gives luminance factors of sparkle spots and luminance factors for backgrounds of elementary areas.

Ferrero et al. introduced three indicators to quantify sparkle distribution of metallic samples [15, 17], and these same quantities can be applied in the case of snow. The first indicator is an illumination contrast C_{sp} which can be computed by illuminance or luminance factors. The illumination contrast of a sparkle spot can be defined for an elementary area by

$$C_{sp} = \frac{\beta_{sp} - \beta_{bg}}{\beta_{bg}} \tag{3}$$

with β_{sp} and β_{bg} luminance factors previously computed. The second indicator is called ensemble contrast of sparkle spots C_E and is defined as the median value of all contrasts of sparkle spots that are above a threshold value C_{th}. For this study case of snow, this quantity C_{th} is evaluated for each patch as the middle of the total range of contrast value computed in the image and follows the definition given by Eq. (4)

$$C_{th} = \frac{C_{sp,\max} + C_{sp,\min}}{2}. \tag{4}$$

The third and last indicator introduced is the density of sparkle spots d_{sp} which represents the number of sparkle spots in the area considered with contrast values C_{sp} higher than the threshold value C_{th}. This value is given in mm^{-2}. As one could expect, this value is linked to the choice of s_{hw} so it is important to choose an area of study large enough to provide a stable statistic for this metric. Among those three indicators presented, only two of them, being the ensemble contrast of sparkle spots C_E and the density of sparkle spots d_{sp}, are used as metrics in this study. The contrast of sparkle spots C_{sp} is indirectly used in the two metrics cited previously.

3. RESULTS

Four descriptors are given in the literature to describe sparkle events happening at the surface of a material: the contrast of sparkle spots, the density of sparkle spots, and their variations due to illumination and viewing conditions. Moreover, with the use of an algorithm to detect sparkle events in digital images, two parameters are introduced: the half-width size s_{hw} for the patch selection and the half-width size of the elementary area l_{hw}. Therefore, a study is conducted to decide on the choice of both parameters s_{hw} and l_{hw}. Once those two parameters for the algorithm are selected, results can be computed. In the dataset, several illumination angles are available as mentioned in Fig. 3. Furthermore, one snow scene was captured from two points of view. Another aspect to study is the type of snow because the age of snow is impacting the size of the snow grain, and images were acquired at different dates, under various illumination conditions (i.e. daylight and artificial light at night).

3.1 *Study of the Algorithm's Parameters*

To adapt the algorithm to the case of this snow dataset, two parameters are introduced: s_{hw} and l_{hw}. In their articles, Ferrero et al. suggested choosing a patch size large enough to ensure materials for the statistics, and the choice of the elementary area l_{hw} was decided to reproduce the circular area visible by a human observer at a distance of 40 cm from the scene in their case. However, they do not provide the values they actually used. Therefore, several values of s_{hw} and l_{hw} are chosen in a given range, and the algorithm is run on part of the dataset to test the influence of those parameters on the resulted contrast and density values.

The patch half-width size is chosen among the following values: 80, 100, 120, 150, and 200 pixels. The range for the elementary area is: 11, 13, 15, 17, and 19 pixels. The algorithm was run 25 times to cover all scenarios on a small part of the dataset to avoid long computation time. Only two scenes from the dataset are considered for showing the results displayed in Figure 4 for the first scene and in Figure 5 for the second scene. Units of the parameters are given in pixels to have a common unit for all images of the dataset. Although the pixel unit could be linked to the resolution of the camera, acquisition setups for all images of the dataset are different. As mentioned, the dataset is composed of images taken with different setups of acquisition. Then, the first images (chronologically speaking) were taken with a setup which has evolved. We do not have the required information for those images to compute the ratio that would link the pixel size to an international unit size such as the meter (or centimeter). To avoid having inhomogeneous data, we therefore chose to not include it here, but it is considered for future works.

From Figs. 4(b) and 5(b), one can notice a variation of density values with the choice of l_{hw} as the linear regression plots are parallel but not superimposed. The smaller this l_{hw} value gets, the larger the density, as it is possible to detect more sparkle spots and have fewer overlaps. However, if l_{hw} gets too small, it does not hold a physical meaning as pointed by Ferrero et al. when they chose it. Similarly, by observing results from Figs. 4(c) and 5(c), contrast values are impacted by the choice of the size of the patch observed s_{hw}. Expanding the size of the patch opens the possibility to detect other sparkle spots and so increases the contrast values as estimated by the algorithm. However, large values of s_{hw} influence the

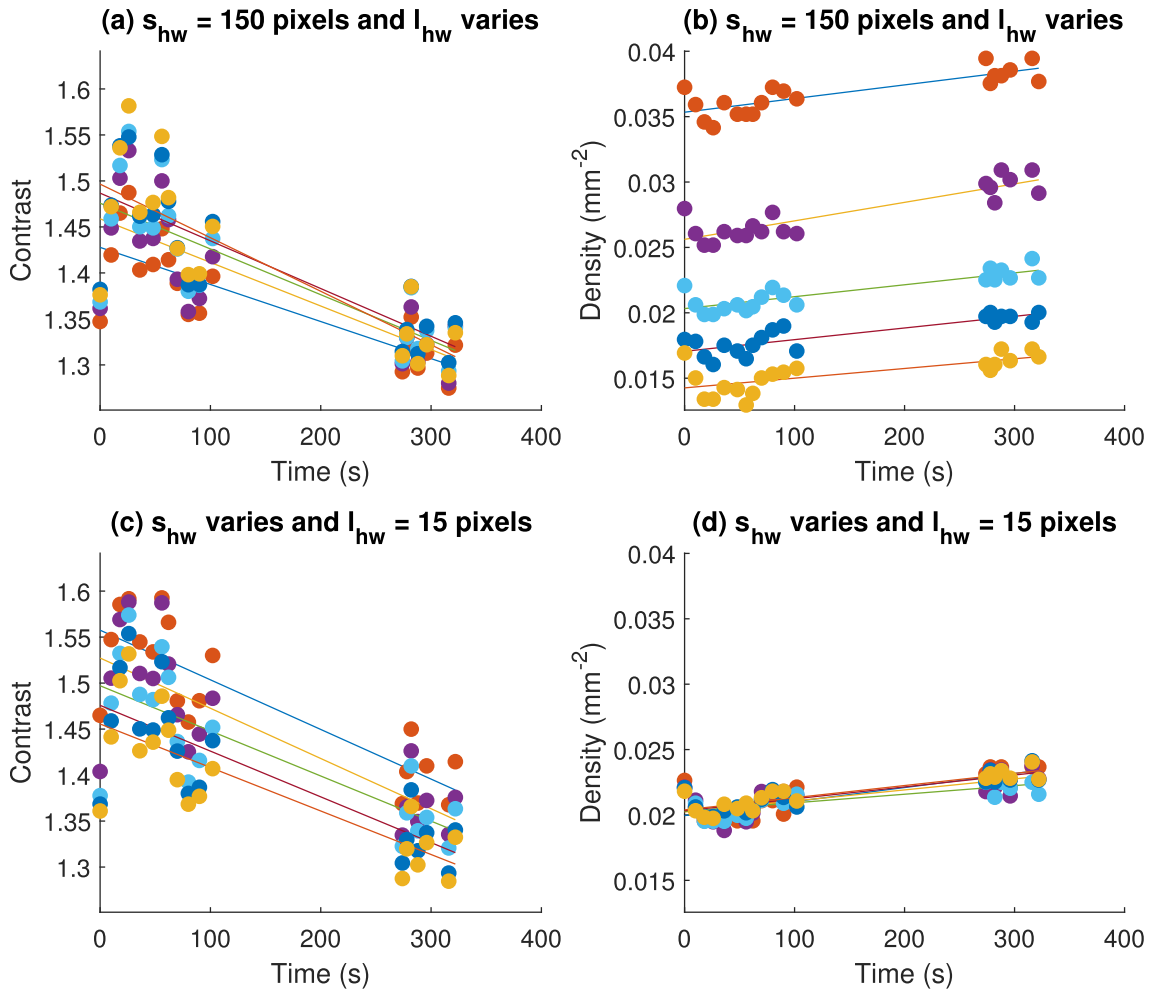

Figure 4. Scatter plots with trend curves resulting from a linear regression; (a) and (b) are obtained by fixing $s_{hw} = 150$ pixels and varying l_{hw}; (c) and (d) are obtained by varying s_{hw} and fixing $l_{hw} = 15$ pixels.

computational time of the algorithm. As a consequence, a trade-off is made in the choice of the size of the elementary area. Ultimately, the values of $s_{hw} = 150$ pixels and $l_{hw} = 15$ pixels are chosen and fixed for the rest of the analysis for the dataset.

3.2 *Influence of the Type of Illumination*

This part tackles the variation in the estimated contrast and density distributions depending on the illumination conditions. One aspect to remind is that day illumination is symbolizing the sunlight, i.e. there was no control over the quantity of light nor the incident angle on the scene. In this study, all images were taken under direct illumination. As mentioned by Kirchner et al. [19], being under direct (no clouds) or diffuse (cloudy overcast sky) illumination highly influences the type of sparkle seen on materials. Azimuth angles for incident light are estimated as explained previously. Regarding night illumination, images were acquired under a torchlight powerful enough to produce sparkle on the snow surface. The algorithm is run on both subsets (day and night) of the dataset to provide contrast and density distributions of sparkle spots.

Figure 6(a) and (b) represent the scatter between the density of sparkle spots (x-axis) and the contrast of sparkle spots (y-axis) respectively for day illumination and night illumination. One thing to note is that the scales for density values are different. The maximum density under daylight is 2.5 mm^{-2} while the maximum density under torchlight at night is close to 0.02 mm^{-2} so a factor of 100 between them. Even though the gap is important, it is relevant to notice that the shape of the scatter clouds looks similar in both cases, and could either be an inverse proportionality function or a decreasing exponential. Our goal is not to estimate this correlation. However, one can note that high contrast values are mostly achieved with small values of densities, while low contrast values are spread in the range of density values. The impact of illumination on density values is massive. High density means there are more sparkle events happening on the surface considered. Under sunlight, it is less surprising to see those high density values. Even though the daylight setups are uncontrolled, the behaviour between contrast and density values remains stable between both illumination modes considered. For the rest of the analysis, the night

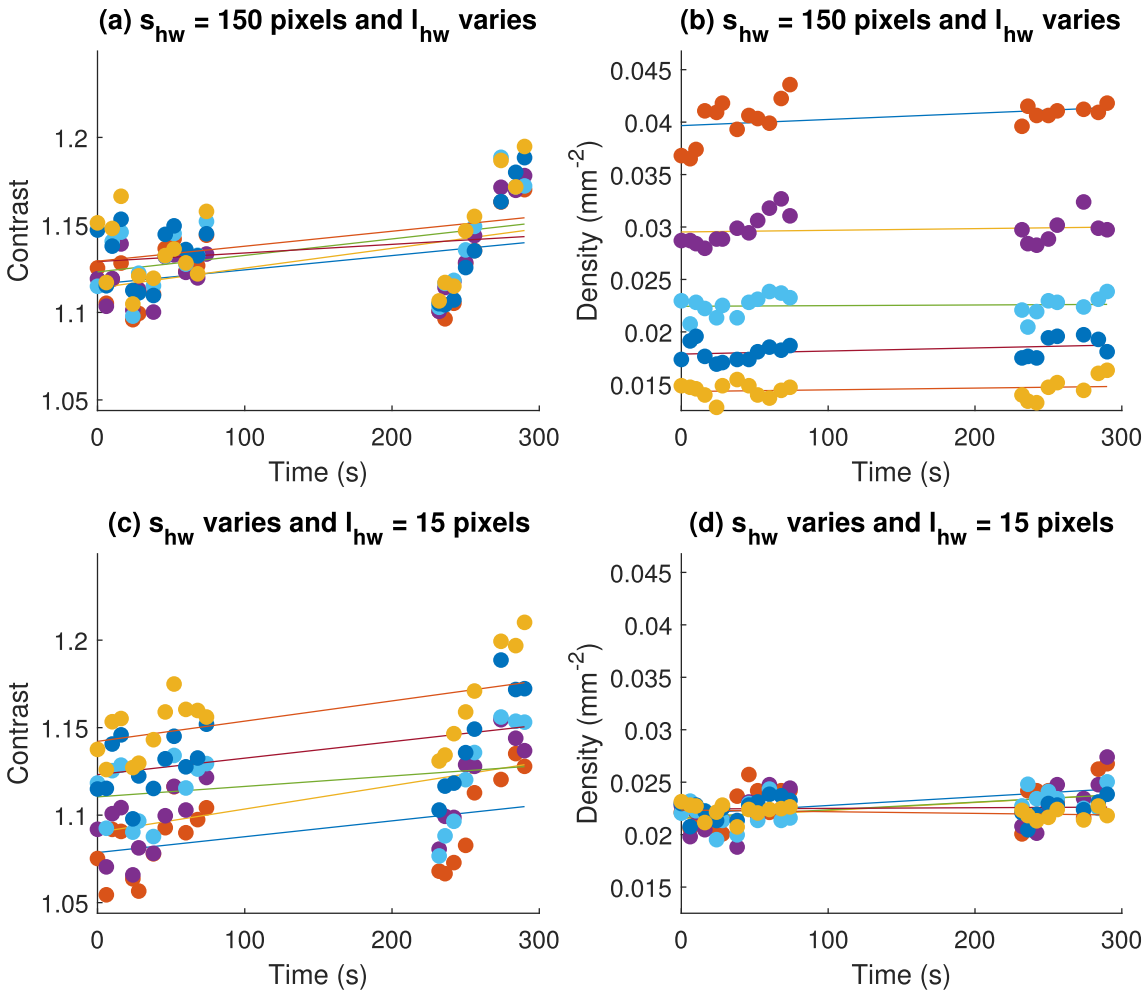

Figure 5. Same configuration as Fig. 4 for another scene observed.

subset is excluded, as it does not hold a lot of images and contains only one type of snow.

3.3 *Influence of the Elevation Angle of the Camera*

In the description of the acquisition of data, two configurations for the position of the camera are mentioned, such as shown in Fig. 2. Therefore, a small study is conducted by separating images taken in the two configurations to check the influence of the elevation angle on the result of contrast and density for sparkle spots.

Figure 7 shows the results obtained for those subsets. For both, the trend for a decreasing exponential or an inverse proportionality function can be observed, even though the scales for contrast and density values are not similar. Since results between the two subsets are quite similar, the distinction on the elevation of the camera is not maintained for the rest of the study. However, the elevation information is to be considered if an experiment is designed to try to identify snow grain shapes.

3.4 *Influence of Type of Snow Observed*

Table I is already presenting the different types of snow composing the dataset and the repartition between images. The reason why the type of snow is important in this study is the link between the type of snow, the age of snow and the grain structure. The age of snow is directly linked to the morphology of the snow grain [1]. When a snow grain is freshly fallen, its size is rather small. Over time and with increasing temperature, it expands and therefore both his size and shape are evolving. Therefore, the older the snow, the bigger the grains with less complex shapes. The shape and size of snow grains should have an interaction with how sparkle events are emitted. Therefore, the aim of this part is to see whether the sparkle spots seen on images are varying with the type of snow.

First, all images used to obtain the results in this part are images taken from the day illumination subset. As stated in Table I, there is a total of 452 images used for the results displayed in Figures 8 and 9. Even though the fresh snow label is in Fig. 8, we chose to add Fig. 9 for a better readability due to smaller scales. Then, as they are now, an accurate description can be made related to the type of snow.

From Fig. 8, the difference made between dense snow (in black) and old snow (in blue) is related to the melting process. Dense snow is an accumulation of fallen snow

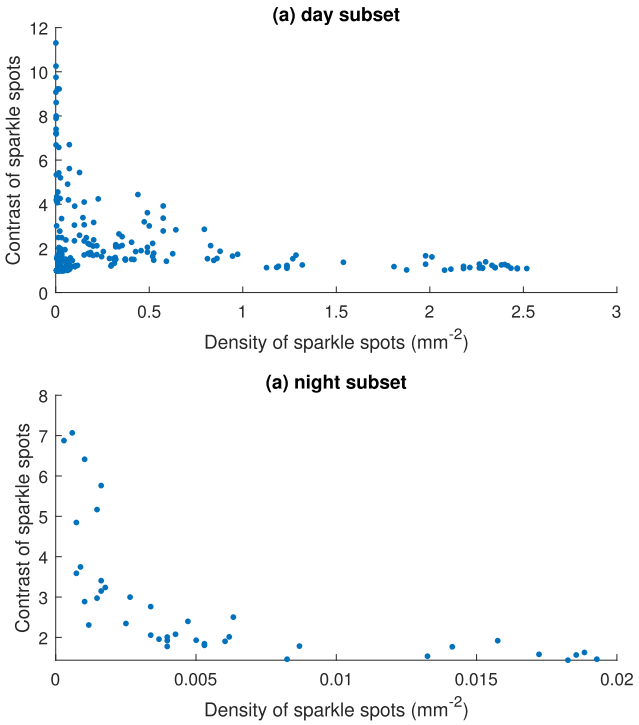

Figure 6. Scatter plots between density of sparkle spots and contrast of sparkle spots for day illumination subset (a) and night illumination subset (b).

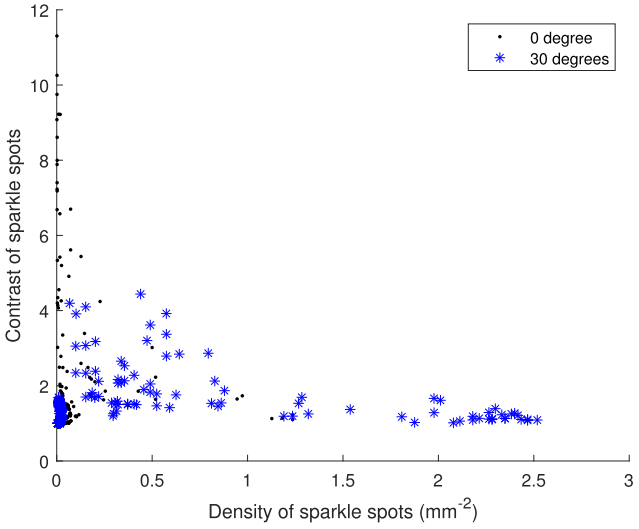

Figure 7. Scatter plot between density of sparkle spots and contrast of sparkle spots for subset of elevation angle of the camera for 0° (black dots) and 30° (blue stars).

grains that could have been accumulated for a long time, hence they could be qualified as old. However, ambient temperature is cold enough to maintain the current state of snow grains. Most of the time, those grains get refrozen due to colder temperature and the wind. For the case of old snow, temperatures are getting above zero degree and then grains are expanding and the transformation from solid to liquid starts. As it can be observed in Fig. 8 with black dots, dense snow tends to produce sparkle with high densities

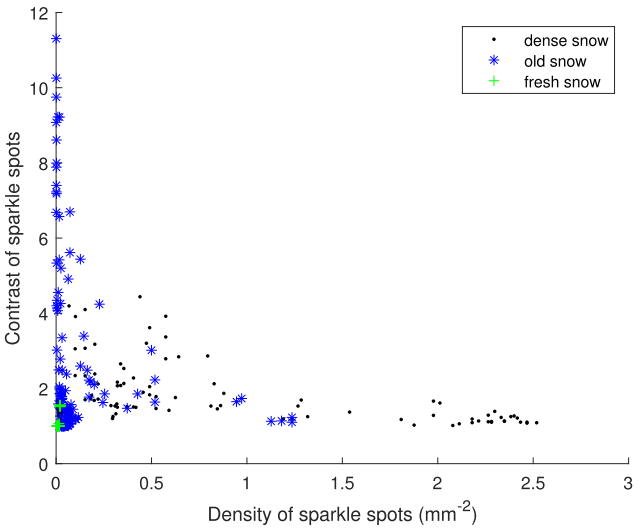

Figure 8. Scatter plot between density of sparkle spots and contrast of sparkle spots for all snow subsets.

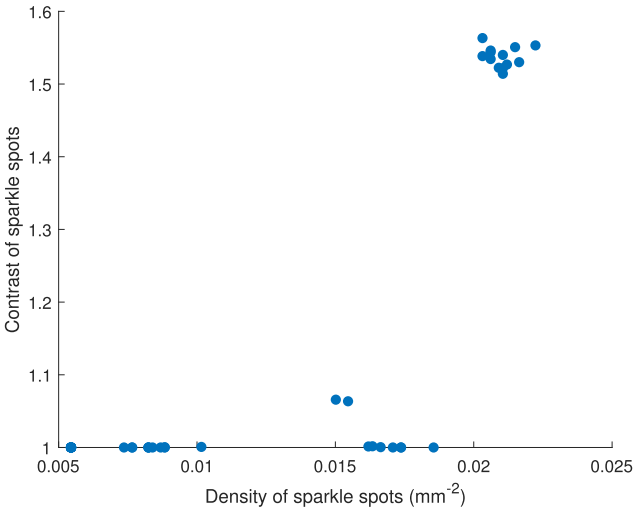

Figure 9. Scatter plot between density of sparkle spots and contrast of sparkle spots for fresh snow subset.

while maintaining contrast values which could be qualified as average. For dense snow as defined here, there are more sparkle spots visible and observable on snow surface even though they remain homogeneous. In the context of old snow, the observation seems to be opposite, as shown in Fig. 8 with blue stars. As opposed to dense snow, older snow whose melting process has started tends to produce sparkle spots with high contrast values and low densities. So, sparkle events may be more visible and shinier on old snow, but they are less likely to happen, or they would be less packed together. Regarding the fresh snow, as illustrated by Fig. 9, it does not involve high contrast values nor density values. Actually, fresh snow is described as snow grains falling on the ground and accumulating quickly. The structure of fresh layer of snow on the surface is not really well-formed, and so fresh snow is less likely to generate sparkles on its surface. However, this conclusion needs to be slightly balanced by

Figure 10. Images from the same snow scene but observed from two points of view.

the small number of images available, only 47 according to Table I.

As a consequence, it is more difficult to see sparkle spots which correlates with low values both for contrast and density: sparkle events are less likely to happen on fresh snow as the snow grains are too small (under 50 μm) and not well-formed. As opposed to fresh snow, dense snow (with snow grain of size around 500 μm and 1 mm) produces a lot of visible sparkles spots and old snow (snow grains above 4–5 mm) generates less sparkle events, but they are more intense.

3.5 *One Snow Scene from Two Points of View*

Some images from the dataset capture the same scene but observed from two different positions. An example of such a scene is displayed in Figure 10.

Then, all images from this particular scene are gathered and studied for their contrast and density of sparkle spots. Since all images are coming from the dense snow subset, performing the analysis on the variation of illumination and viewing conditions on a similar scene may provide some information related to the geometry and the shape of snow grains.

Figures 11 and 12 display the results obtained for the contrast and density of sparkle spots for this study case. These results are presented differently from the previous ones. Here, it is more interesting to focus on the variations of contrast and density due to different viewing conditions. The camera is looking at the same scene under two perspectives. Hence, snow grains remain constant in the scene, but their effect vary with the viewing conditions. Both radial plots in Figs. 11 and 12 are results correlated to the estimated azimuth angle of the sun on images. On the left image of Fig. 10 (chosen as a reference for the reference system), one can notice shadows cast from the tripod of the camera. Using these shadows, the angle is estimated to 30° and then 210° for its counterpart. The angles displayed on the radial plots are the relative azimuth angle between the camera and the light source.

Focusing on the radial scatter plots, the interesting aspect to notice is that contrast and density values do not vary much even though sparkle spots are observed from a different viewing angle. This statement is also supported by looking to the shapes of contrast and density distributions. Even though the number of images used (66) is not large enough to make statistical estimations, the shapes of unimodal distributions can be distinguished. More accurately, distributions seem to have a centered value and other values dispatched around it. It can be interpreted as it follows: contrast and density values accumulate towards one average value in a range controlled by a small standard deviation.

A reason why such results can be observed could be correlated to the randomness of the distribution of snow grains onto the snow sample considered. Due to this randomness, potential effects due to geometry of snow grains would be averaged and therefore have less impact. However, if we assume the distribution could be estimated, another reason would then be the shape of the snow grains. In fact, it could even give information on the shape. If one assumes a spherical shape for a grain, then such a grain would reflect light the same way in all possible directions. Then, regardless of the viewing conditions, sparkle spots would have a small variation and could remain stable while the camera rotates around the scene. Due to the lack of number of viewing positions for this scene, it is impossible to conclude accurately on the type of the shape. However, it opens possibilities for designing an acquisition protocol to do so. By selecting one single snow scene and fixing the illumination conditions, several captures can be performed at various positions around the scene. Then, similar radial scatter plots can be obtained, and by observing potential symmetries, one might conclude on the nature of the grain shape.

4. CONCLUSION

In this article, multiple statistical studies on sparkle from snow are computed on a dataset of images acquired *in-situ*. The dataset covers various types of snow and several illumination and viewing conditions. Two indicators are considered in this study: contrast values and density values of sparkle spots. The dataset was mainly divided in three subsets correlated to the type of snow. By observing those three clusters of the dataset, we show it is possible to link the results of the sparkle to the structure of snow.

Fresh snow is composed of very small and fine grains whose crystal structure has yet to be formed. As such, the likelihood of observing sparkle events on fresh snow is very low. Dense snow is defined by snow grains fully formed, with varying shapes and sizes less than a millimeter.

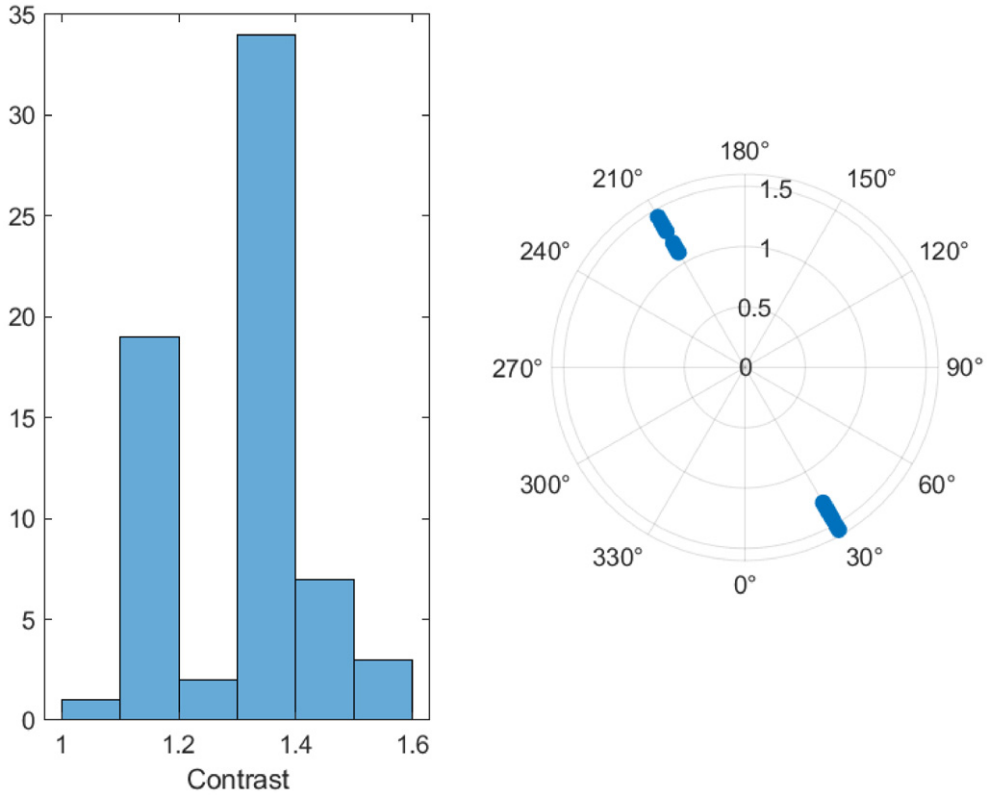

Figure 11. (Left) Contrast of sparkle spots distribution. (Right) Variation of contrast depending on viewing conditions.

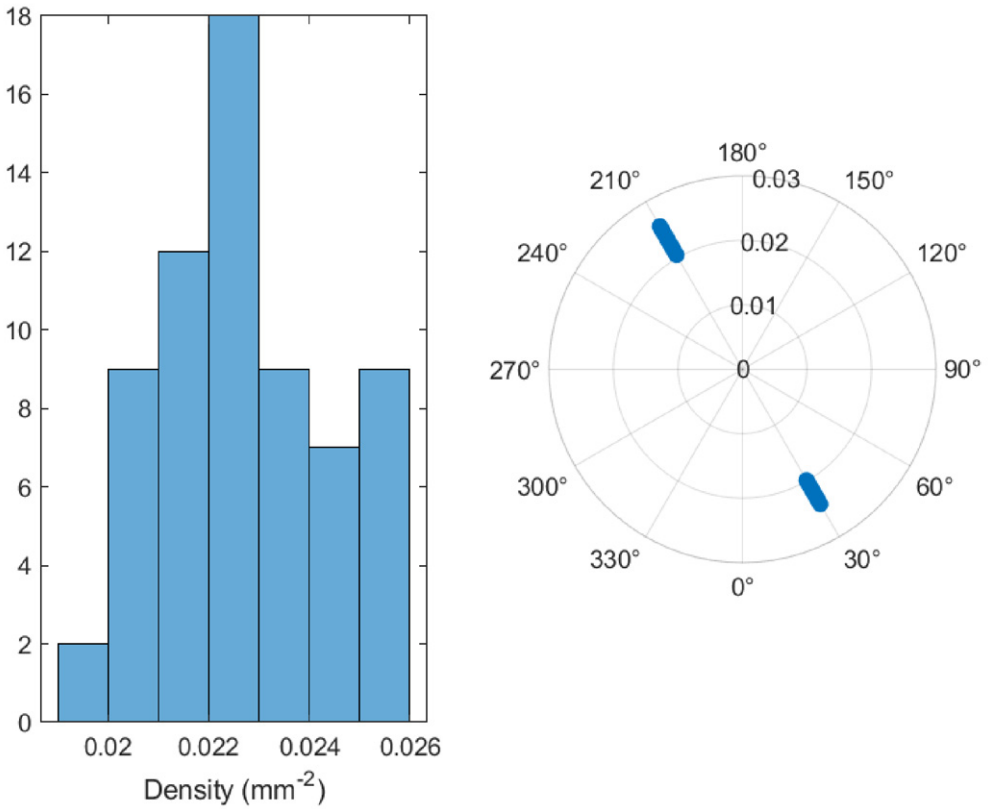

Figure 12. (Left) Density of sparkle spots distribution. (Right) Variation of density depending on viewing conditions.

Most importantly, dense snow is observed in a cold environment. So, when illumination conditions are met, one can experience numerous homogeneous sparkle events occurring on the surface of dense snow. Finally, old snow is mainly dense snow in a warmer environment so that the melting process has started. Snow grains are then expanding and sparkles are observable in a smaller number but may be more intense as well.

Results and interpretations between sparkle events and the snow open possibilities for future work. Although it has been extensively used for car paintings and metallic materials, the method to detect and estimate the sparkle on snow has been tested and proved, and it can be linked to the snow structure. From this observation, we consider conducting an experiment of a larger scale that aims to relate more precisely the grain size and shape to the indicators of sparkle. This experiment should enable the use of sparkle measurement as a powerful tool to classify snow grains. Other possibilities for applying such a method could be to study the glint effect on water surface from sea or rivers, or to estimate dust particles sizes when taking underwater pictures.

REFERENCES

[1] C. Fierz, R. Armstrong, Y. Durand, P. Etchevers, E. Greene, D. McClung, K. Nishimura, P. Satyawali, and S. Sokratov, "The International classification for seasonal snow on the ground," *Technical Documents in Hydrology* (UNESCO/IHP, Paris, 2009).

[2] G. Picard, L. Arnaud, F. Domine, and M. Fily, "Determining snow specific surface area from near-infrared reflectance measurements: Numerical study of the influence of grain shape," Cold Reg. Sci. Technol. **56**, 10–17 (2009).

[3] Q. Libois, G. Picard, J. France, L. Arnaud, M. Dumont, C. Carmagnola, and M. King, "Influence of grain shape on light penetration in snow," The Cryosphere **7**, 1803–1818 (2013).

[4] L. Leppänen, A. Kontu, J. Vehviläinen, J. Lemmetyinen, and J. Pulliainen, "Comparison of traditional and optical grain-size field measurements with SNOWPACK simulations in a taiga snowpack," J. Glaciol. **61**, 151–162 (2015).

[5] R. Pirazzini, P. Räisänen, T. Vihma, M. Johansson, and E.-M. Tastula, "Measurements and modelling of snow particle size and shortwave infrared albedo over a melting Antarctic ice sheet," The Cryosphere **9**, 2357–2381 (2015).

[6] M. Nguyen, J.-B. Thomas, and I. Farup, "Investigating the Kokhanovsky snow reflectance model in close range spectral imaging," *Proc. IS&T CIC29: Twenty-Nineth Color and Imaging Conf.* (IS&T, Springfield, VA, 2021), pp. 31–36.

[7] A. Kokhanovsky and F.-M. Breon, "Validation of an analytical Snow BRDF model using PARASOL multi-angular and multispectral observations," IEEE Geosci. Remote Sens. Lett. **9**, 928–932 (2012).

[8] B. Wang and H. Bowles, "A robust and flexible real-time sparkle effect," *Proc. Eurographics Symposium on Rendering: Experimental Ideas & Implementations* (EUROGRAPHICS Association, Geneve, 2016).

[9] W. Jakob, M. Hasan, L.-Q. Yan, J. Lawrence, R. Ramamoorthi, and S. Marschner, "Discrete stochastic microfacet models," ACM Trans. Graph. **33**, 1–10 (2014).

[10] B. Wang, H. Deng, and N. Holzschuch, "Real-time glints rendering with pre-filtered discrete stochastic microfacets," Comput. Graph. Forum **39**, 144–154 (2020).

[11] *ASTM E284-17, Standard Terminology of Appearance,* ASTM International, West Conshohocken, PA, 2017.

[12] S. Ershov, A. Khodulev, and K. Kolchin, "Simulation of sparkles in metallic paints," *Proc. Graphicon, Int'l. Conf. Graphicon* (Dialog-MSU, Moscow, 1999).

[13] S. Kitaguchi, S. Westland, R. Luo, E. Kirchner, and G. Kieboom, "Application of HDR imaging to modeling of glints in metallic coatings," *Proc. AIC 2008 Interim Meeting Colour - Effects & Affects* (AIC, Stockholm, 2008).

[14] A. Ferrero, J. Campos, A. Rabal, and A. Pons, "A single analytical model for sparkle and graininess patterns in texture of effect coatings," Opt. Express **21**, 26812–26819 (2013).

[15] A. Ferrero and S. Bayon, "The measurement of sparkle," Metrologia **52** (2015).

[16] A. Ferrero, N. Basic, J. Campos, M. PastuscheK, E. Perales, G. Porrovecchio, M. Smid, A. Schirmacher, J. Velázquez Molinero, and F. Martínez-Verdú, "An insight into the present capabilities of national metrology institutes for measuring sparkle," Metrologia **57** (2020).

[17] A. Ferrero, E. Perales, N. Basic, M. Pastuschek, G. Porrovecchio, A. Schirmacher, J. Velázquez Molinero, J. Campos, F. Martinez-Verdú, M. Smid, T. Dauser, P. Blattner, and P. Linduska, "Preliminary measurement scales for sparkle and graininess," Opt. Express **29**, 7589–7600 (2021).

[18] N. Kwok, D. Wang, K. Jia, S. Chen, G. Fang, and Q. Ha, "Gray world based color correction and intensity preservation for image enhancement," *2011 4th Int'l. Congress on Image and Signal Processing* (IEEE, Piscataway, NJ, 2011), Vol. 2, pp. 994–998.

[19] E. Kirchner, G.-J. van den Kieboom, L. Njo, R. Supèr, and R. Gottenbos, "Observation of visual texture of metallic and pearlescent materials," Color Res. Appl. **32**, 256–266 (2007).